HTS/FTIR investigations in the spectral range 4000–600 cm−1 and BET method of specific surface area of various montmorillonite clays modified by monocationic and dicationic imidazolium ionic liquids

A. Ahmed, W.A.A. Ahmed, T. Moumene, El Belarbi, V. Baeten, Serge Bresson

Chemical Physics 598 (2025) 112844

Contents lists available at ScienceDirect

Chemical Physics

journal homepage: www.elsevier.com/locate/chemphys

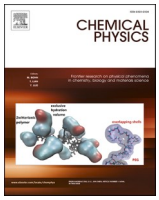

HTS/FTIR investigations in the spectral range 4000–600 cm^{-1} and BET method of specific surface area of various montmorillonite clays modified by monocationic and dicationic imidazolium ionic liquids

A. Ahmed [a], W.A.A. Ahmed [a], T. Moumene [b], El H. Belarbi [b], V. Baeten [c], S. Bresson [d,*]

[a] Department of Physics, Faculty of Science, Sabratha University, Libya
[b] Laboratoire Synthèse et Catalyse, Ibn Khaldoun University, Tiaret, Algeria,
[c] Walloon Agricultural Research Centre (CRA-W), Valorisation of Agricultural Products, Department, Food and Feed Quality Unit (U15), 'Henseval Building', Chaussée de Namur 24, 5030 Gembloux, Belgium
[d] Institut Polytechnique UniLaSalle, Université d'Artois, ULR 7519, 19 Rue Pierre Waguet, BP 30313, 60026 Beauvais, France

ARTICLE INFO

Keywords:
Montmorillonites KSF
K10
SWy-3
Monocationic and dicationic liquids
Ionic liquids
HTS/FTIR spectroscopy
BET method

ABSTRACT

Three different types of montmorillonite, K10, KSF, and SWy-3, were analyzed using HTS/FTIR spectroscopy. The HTS/FTIR spectra revealed two spectral regions (3800–2600, 2000–1000 cm^{-1}), highlighting the vibrational signatures that differentiate the three types of clays. The vibrational study of the three types of clays modified with two ionic liquids ($[EMIM^{+}][I^{-}]$ monocationic ionic liquid and $[M(CH_2)IM^{2+}][2I^{-}]$ dicationic ionic liquid) revealed several vibrational changes directly related to the presence of the ionic liquids in the clays. On one hand, the transition from monocationic to dicationic ionic liquids intercalated into the clay structure significantly affected the HTS/FTIR spectra. On the other hand, the HTS/FTIR spectra of SWy-3 show more significant vibrational changes than those of the other two clays after the intercalation of ionic liquids. To complement these results, a study of the specific surface area of these clays and these clays modified by the $[M(CH_2)IM^{2+}][2I^{-}]$ dicationic ionic liquid using the BET method is presented.

1. Introduction

Montmorillonite is a clay mineral belonging to the smectite group. It forms through the weathering or alteration of volcanic ash in the presence of water. Its 2:1 layered structure consists of a central octahedral sheet of alumina sandwiched between two tetrahedral sheets of silica. This very soft phyllosilicate mineral has the chemical formula $(Na,Ca)_{0.3}(Al,Mg)_2Si_4O_{10}(OH)_2n(H_2O)$ [1].

Montmorillonite (MMT) contains negative charges that are balanced by inorganic cations, such as Na^{+}, Ca^{2+}, and Mg^{2+}. These exchangeable cations make MMT an effective adsorbent for various cationic contaminants, particularly in wastewater treatment. Additionally, MMT possesses unique properties, including a large surface area, high cation exchange capacity, and swelling ability, which further enhance its adsorption efficiency [2]. The layered structure of montmorillonite allows water to easily penetrate the interlayer spaces between layers, causing the clay to swell significantly. This property makes montmorillonite highly effective in sealing and water barrier applications [3]. Due to these unique properties, montmorillonite has been the subject of extensive research.

Ionic liquids (ILs) are compounds that have transformed research and chemical industries in recent years. As key players in the green chemistry revolution, these solvents significantly reduce the use of hazardous, toxic, and environmentally harmful substances [4]. Ionic liquids (ILs) are generally defined as liquid electrolytes composed entirely of ions. As novel green solvents, they are made up of organic cations and organic or inorganic anions, forming salts that are liquid at or below room temperature. Their melting points are typically below 100 °C [5,6]. The melting temperature and solubility properties of an ionic liquid depend on both its cation and anion. By varying either the cation or the anion, they are typically composed of a cation (often organic, such as imidazolium, pyridinium, or phosphonium) and an anion (such as bis(trifluoromethylsulfonyl)imide, tetrafluoroborate, or hexafluorophosphate) [5,6].

Imidazolium-based ionic liquids offer remarkable versatility, owing to their excellent thermal stability, low volatility, and wide solubility

* Corresponding author.
E-mail address: sergebresson@yahoo.fr (S. Bresson).

https://doi.org/10.1016/j.chemphys.2025.112844
Received 19 May 2025; Received in revised form 21 June 2025; Accepted 2 July 2025
Available online 7 July 2025

range. By modifying their structure and immobilizing them on clay surfaces, they enhance interlayer spacing, increase hydrophobicity, and enable selective molecular interactions. These improvements expand the potential applications of clay-based materials in various fields [7].

Monocationic and dicationic imidazolium ionic liquids serve as important modifiers for clays, each offering distinct structural and functional benefits. Monocationic ILs, containing one imidazolium cation, are valued for their simplicity and ease of functionalization. In contrast, dicationic ILs, composed of two imidazolium groups connected by a spacer, provide superior thermal stability, stronger interlayer bonding, and enhanced mechanical properties. These advantages make dicationic ILs particularly well-suited for more advanced and demanding applications [8,9].

To replace activated carbon in the treatment of wastewater from industries or polluted soils with natural-origin products such as clays, new families of microporous solids with controlled porosity, known as modified clays, have gained renewed interest through the use of ionic liquids as intercalation compounds [10–12]. A. Ahmed et al. [8] demonstrated that it is possible to intercalate two different ionic liquids, the monocationic ionic liquid $[EMIM^+][I^-]$ and the dicationic ionic liquid $[M(CH_2)IM^{2+}][2I^-]$, into three montmorillonites (K10, KSF, and SWy-3) through X-ray diffraction studies. Indeed, they show that for these modified clays, the reflection peaks 2θ (°) of the (001) plane displaced toward lower values as a result of the intercalation process of ionic liquids in the clay, in accordance with Bragg's law. These authors also highlighted the impact of these two ionic liquids on the vibrational modes of these modified clays in the spectral regions of 3700–3100 cm^{-1} and 1750–1600 cm^{-1} through ATR/FTIR studies.

Fourier Transform Infrared (FTIR) spectroscopy is an essential and versatile technique commonly used to examine molecular structures and chemical interactions. Among its key variations, Attenuated Total Reflectance FTIR (ATR-FTIR) and High-Throughput Screening FTIR (HTS-FTIR) stand out, each offering unique advantages for material analysis. ATR-FTIR is particularly effective for analyzing surfaces with minimal sample preparation, making it ideal for single-sample investigations. Conversely, HTS-FTIR offers exceptional efficiency for processing large numbers of samples, significantly improving throughput and reducing analysis time compared to traditional ATR-FTIR [13]. Together, these complementary methods enable researchers to tackle a wide range of analytical challenges accurately and efficiently [13]. In the context of clay modification, especially for montmorillonite, HTS-FTIR is particularly effective in analyzing interactions between interlayer ions and modifying agents, such as ionic liquids. It can identify even minor chemical alterations and help optimize modification processes in a time-efficient manner [8,14]. The HTS/FTIR spectroscopy technique offers advantages over ATR/FTIR. In Fig. 1, we present our obtained spectra of SWy-3 MMT, a smectic clay from Wyoming (USA) that is rich in Na, by ATR/FTIR and HTS/FTIR spectroscopy. We note that, compared to the ATR/FTIR technique, HTS/FTIR spectroscopy highlights weak-intensity spectral regions that were less detectable in ATR spectra. Indeed, compared to the ATR/FTIR spectrum, where the spectral region 1300–700 cm^{-1} dominates in intensity, the spectral regions 4000–2700 and 2000–1000 cm^{-1} are much more pronounced in the HTS/FTIR spectrum, which should facilitate spectral analysis in these regions. HTS provided greater sensitivity to absorption in this spectral range, allowing the discovery of new differentiation parameters between clays themselves and between clays intercalated with monocationic and dicationic ionic liquids.

First, a study of the specific surface area of these clays and their modified forms using the BET method aims to determine the best choice of modified clays for capturing pollutants through the intercalation of ionic liquid within the clay. Indeed, the modification of the clay surface using ionic liquids allows for the expansion of the interlayer volume of the clay mineral sheets, imparting hydrophobic and organophilic properties, and thereby increasing their potential for the adsorption of certain hazardous pollutants present in water or wastewater that has

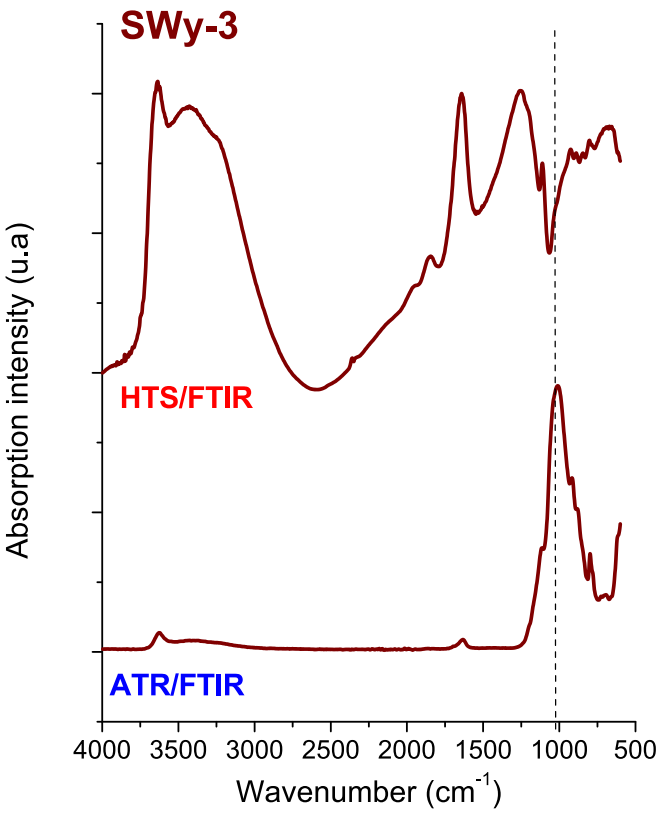

Fig. 1. Comparison of the obtained spectra of SWy-3 MMT using ATR/FTIR and HTS/FTIR spectroscopy. The black dashed line indicates the mode at 1000 cm^{-1}, which was used as the reference for spectrum normalization in the ATR/FTIR spectrum.

undergone conventional preliminary treatment. Secondly, HTS-FTIR analyses are performed to complete and refine this same study using ATR/FTIR [8] in more precisely defined spectral regions by investigating the intercalation of K10, KSF, and SWy-3 montmorillonites with two distinct imidazolium-based ionic liquids. These ionic liquids, synthesized in our laboratory, include a monocationic ionic liquid, $[EMIM^+][I^-]$, composed of a cation, 1-ethyl-methylimidazolium ($C_6H_{11}N_2^+$), and an iodide anion, and a dicationic ionic liquid, $[M(CH_2)IM_2^+][2I^-]$, composed of two cations defined by two imidazolium groups attached via a methylene bond (CH_2) and two iodide anions.

2. Materials and methods

2.1. Montmorillonites

The K10 and KSF montmorillonites were supplied by Sigma-Aldrich, while the SWy-3 Na-rich montmorillonite was obtained from Clay Minerals (Aurora, USA). The K10 and KSF montmorillonites are obtained through a treatment of montmorillonites with sulfuric acid. The difference between these two clays lies in the intensity of the treatment. For KSF, the sulfuric acid treatment is milder than for K10.

The effect of sulfuric acid attack on the physicochemical properties of the clays depends on the treatment conditions (acid concentration, temperature, contact time, etc.). The attack of the clay by the acid follows a mechanism that begins with the adsorption of sulfuric acid on the clay surface, leading to the substitution of exchangeable ions. Thus, the structural cations of the clay (Al^{3+}, Mg^{2+}, Fe^{3+}) are replaced, during the acid attack, by protons (H^+), resulting in a substantial increase in the surface acidity of the clay.

In K10 montmorillonite, Na is present in very small amounts: less than 0.3 % by weight relative to the total constituents (SiO_2: 79.6 %;

Al_2O_3: 15.1 %; K_2O: 1.6 %; MgO: 1.5 %; CaO: 0.4 %; Fe_2O_3: 1.4 %; TiO_2: 0.3 %) [15]. For the KSF montmorillonite produced by Aldrich, the composition is quite different: SiO_2: 53.35 %; Al_2O_3: 18.8 %; H_2SO_4: 6 %; MgO: 2.8 %; CaO: 2.9 %; Fe_2O_3: 5.1 %; 8.1 % lost on ignition [15]. It is noteworthy that the milder sulfuric acid treatment used for KSF montmorillonite leads to a higher proportion of structural cations (Al^{3+}, Mg^{2+}, Fe^{3+}) and Ca^{2+} in its chemical composition compared to K10 montmorillonite. Both of these clays are cationic acids.

Wyoming-type montmorillonite is a type of montmorillonite characterized by a small negative net charge of approximately −0.35 to −0.85 per $O_{20}(OH)_4$, with tetrahedral substitutions contributing −0.15 to −0.50 of the total charge and specific thermal properties [16]. Thus, SWy-3 montmorillonite is an anionic acid and is also enriched in sodium (Na), as shown by its chemical composition: SiO_2: 62.9 %; Al_2O_3: 19.6 %; K_2O: 0.53 %; MgO: 3.05 %; CaO: 1.68 %; Fe_2O_3: 3.35 %; FeO: 0.32 %; TiO_2: 0.09 %; Na_2O: 1.53 % [15].

In conclusion, K10 montmorillonite has the highest silicon content compared to KSF and SWy-3 MMTs but the lowest levels of structural cations (Al^{3+}, Mg^{2+}, Fe^{3+}) and Ca^{2+} cations, with virtually no Na^+ cation present. KSF montmorillonite appears to fall between K10 and SWy-3, with intermediate levels of Al^{3+}, Mg^{2+}, and Fe^{3+} cations, but a maximum level of Ca^{2+} cation. On the other hand, SWy-3 montmorillonite is characterized by a high level of Na^+ cation and its anionic behavior.

XRD analyses of K10, KSF, and SWy-3 montmorillonites, without further treatment, revealed the presence of various impurities (see Fig. 2). The improvements in the diffraction diagram are clearly visible, notably the elimination of certain peaks corresponding to impurities. Prior purification was necessary to extract the clay fraction. The clays were purified following the experimental method detailed in the article published by Haouzi et al. [17].

Clay purification was carried out according to the following experimental protocol:

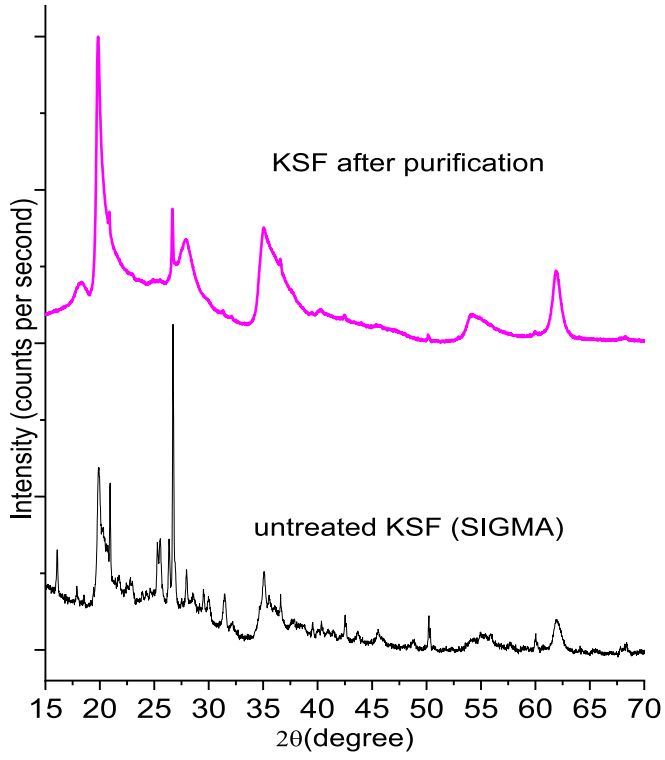

Fig. 2. XRD diffraction of KSF untreated and purified KSF with wide angles, 15–70°.

- **Preparation of the suspension:**
  Twenty grams (20 g) of raw clay were dispersed in one liter (1 L) of distilled water, with the addition of a few drops of sodium hydroxide (NaOH) to promote particle deflocculation.
- **Agitation:**
  The mixture was mechanically stirred at 300 rpm for two hours at room temperature (25 °C) to ensure good dispersion of the fine particles.
- **Decantation:**
  The resulting suspension was then transferred into a 1 L graduated cylinder and left to rest for 24 h. This step allows the sedimentation of the coarser particles, while the montmorillonite remains in suspension.
- **Recovery of the colloidal phase:**
  Approximately 400 mL of the upper phase, mainly containing fine particles (montmorillonite), was carefully collected.
- **Centrifugation:**
  The collected phase was subjected to centrifugation to separate the clay particles from the liquid phase.
- **Drying and grinding:**
  The obtained precipitate was dried at a temperature above 100 °C, then finely ground to obtain a homogeneous powder. This step allowed the recovery of approximately 1 g of purified montmorillonite.

2.2. Synthesis of ionic liquids

The synthesis of $[M(CH_2)IM^{2+}][2I^-]$ dicationic ionic liquid was performed as per Moumene et al. [9]. The synthesis of $[EMIM^+][I^-]$ monocationic ionic liquid was performed as per Noack et al. [18].

2.3. Intercalation of ionic liquid into MMT

An amount of 5 g of MMT and 5 g of ionic liquids were mixed into 250 mL of distilled water and shaken on a mechanical shaker with horizontal agitation at 400 rpm for 24 h at room temperature. The mixtures were then centrifuged at 5000 rpm for 2 min, and the supernatants were passed through 0.45 µm filters before being analyzed by HTS/FTIR instruments. The percentage of the ionic liquid volume incorporated relative to the volume of the clay particles can be estimated by comparing the interlayer distances of the raw clay and the modified clay, assuming that the surface areas of the galleries between the layers remain practically unchanged, and that the increase in the volume of the purified clay exchanged with the ionic liquid results from the expansion of the interlayer spacing.

The formula is:

$$\%of\ incorporated\ ionic\ liquid\ relative\ to\ the\ total\ volume = \frac{(d_2 - d_1)}{d_1}$$

where d_1 is the interlayer distance of the pure clay, and d_2 is the interlayer distance of the clay modified with the ionic liquid [8]. Table 1 shows the corresponding percentages for the clays and ionic liquids investigated.

2.4. HTS/FTIR analyses

FT-IR spectra were recorded on a VERTEX 70 spectrometer coupled with a microplate reader HTS-XT extension (BRUKER, Ettlingen, Germany). Approximately 30 mg of purified clays or clays modified by ionic liquids were placed on IR-transparent Zn-Se microtiter plates with 96 wells (Bruker Optics, Germany). Each sample was analyzed in duplicate, meaning two MIR spectra were recorded from two independent 30-mg samples. The mid-infrared (MIR) spectra were obtained by averaging 64 scans in the spectral range between 4000 and 600 cm^{-1} at a resolution of 4 cm^{-1}, with 64 spectra co-added. Data were processed using

Table 1
percentages of incorporated ionic liquid relative to the total volume. [8].

	Interlayer		Distance (Å)		%of incorporated	ionic liquid
	Pure clay	Clay + [EMIM$^+$][I$^-$]	Clay + [M(CH$_2$)IM^{2+}][2I$^-$]	Pure clay	Clay + [EMIM$^+$][I$^-$]	Clay + [M(CH$_2$)IM^{2+}][2I$^-$]
K10	11.74	12.79	13.1	0	8.20	10.38
KSF	11.28	12.93	12.93	0	12.76	12.76
Swy-3	10.95	12.87	13.11	0	14.91	16.47

the OPUS 6.5 software (Bruker Optics).

2.5. Specific surface area measurement by BET

The specific surface area measurements for our samples were carried out at the Laboratory of Reactivity and Solid Chemistry (LRCS), University of Picardie Jules Verne, in Amiens, France. To measure the specific surface area using the BET method, it is necessary to degas the samples at a temperature close to their boiling point in order to remove the adsorbed water, making the surfaces of the material available to nitrogen molecules (N_2), which is the gas used for our experiments. The clay and modified clay samples (approximately 100 mg) were first degassed at 150 °C under vacuum for 3 h before measurement. The analysis of a nitrogen adsorption point at 77 K was determined to obtain the BET specific surface area using a Porosimeter-type device (Micromeritics ASAP 2020).

Among the two ionic liquids studied, only the [M(CH$_2$)IM^{2+}][2I$^-$] dicationic liquid has a melting point higher than 150 °C [9]. For the monocationic ionic liquid, the melting point is observed at 74.5 °C [9]. However, before conducting BET studies, we need to perform a degassing under vacuum at 150 °C to remove the water adsorbed by our samples. Therefore, we will observe modifications in the molecular structures of the clay samples modified by the monocationic ionic liquid, which could distort the BET results. Thus, only the clays modified by the dicationic liquid will be studied using the BET method.

2.6. Statistical analysis

To refine our study, we performed modeling of infrared spectra using Lorentzian functions to determine the wavenumber values and the areas of the associated peaks. The mode frequencies were obtained through modeling conducted with ORIGIN 5.0 Professional software. The modeling method was proposed by Bresson et al. [14]. We used the following Lorentzian function as the peak function:

$$y = y_0 + \frac{2A}{\pi}\cdot\frac{w}{4(x-x_c)^2 + w^2}$$

where x_c represents the wavenumber of the fitted mode, AAA the area of the peak, and www the width at half-height. We performed 100 iterations, with an estimated error of ±0.5 cm^{-1}.

3. Results and discussion

3.1. Comparison of the specific surface areas by the BET method of K10, KSF, and SWy-3 MMTs and the clays modified by the [M(CH$_2$)IM^{2+}][2I$^-$] dicationic ionic liquid

3.1.1. Cases of K10, KSF, and SWy-3 MMTs

The nitrogen adsorption-desorption isotherms for K10, KSF, and SWy-3 using the BET method are shown in Figs. 3a and b.

From Fig. 3.a, it is observed that for the three montmorillonites, the isotherms are of type IV, with a hysteresis loop of type H4, according to the IUPAC classification [19]. The type IV isotherm is characteristic of porous adsorbents with pore sizes ranging from 15 to 100 Å. On the other hand, the hysteresis loop of type H4 is indicative of solids with small pore size distributions.

The results obtained by the BET method for K10, KSF, and SWy-3 are presented in Table 2. The specific surface areas are 280, 97, and 45 m^2/g

Table 2
Results obtained by the BET method on purified K10, KSF, and SWy-3 montmorillonites (S_{BET} = BET specific surface area and V = Pore volumes).

Clays	S_{BET} (m^2/g)	V_{pores} (cm^3/g)	d_{pores}(nm)
K10	280 ± 1	0.39 ± 0.01	3.90 ± 0.02
KSF	97 ± 1	0.15 ± 0.01	3.94 ± 0.02
SWy-3	45 ± 1	0.09 ± 0.01	3.71 ± 0.02

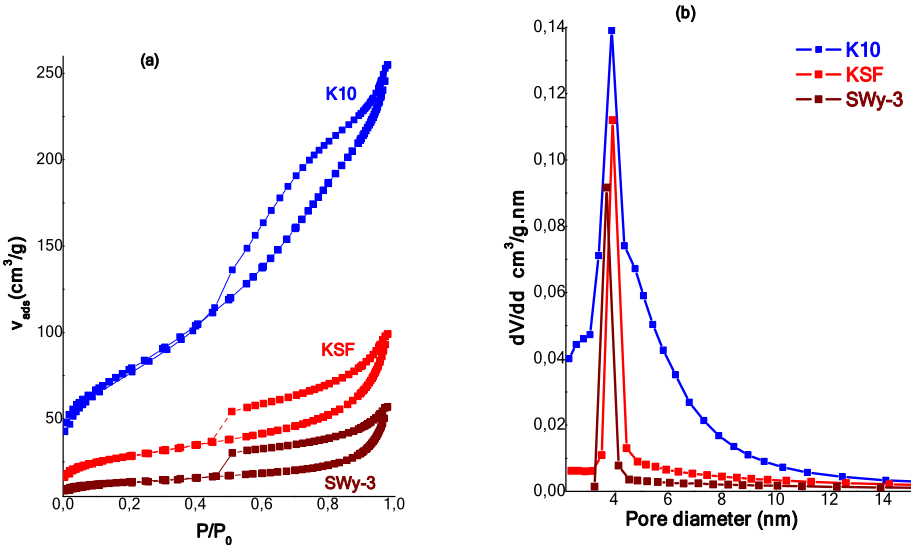

Fig. 3. Adsorption-desorption isotherms for K10, KSF, and SWy-3 MMTs (a) and pore size distribution for K10, KSF, and SWy-3 MMTs (b).

for K10, KSF, and SWy-3, respectively, while the pore volumes are 0.39 cm^3/g for K10, 0.15 cm^3/g for KSF, and 0.09 cm^3/g for SWy-3.

Thus, it is observed that montmorillonite K10 has a significantly higher adsorption capacity compared to KSF or SWy-3: nearly three times the adsorption capacity compared to KSF and six times that of SWy-3. These measurements are consistent with those provided in the literature: for untreated K10, Aldrich reports a specific surface area between 200 and 250 m^2/g, and S. Kawi et al. estimate the specific surface area of their K10 montmorillonite to be 197 m^2/g [19]; for KSF, Aldrich recommends a specific surface area between 20 and 40 m^2/g; and finally, "Physical and Chemical Data of Source Clays" estimates the specific surface area of SWy-3 to be 32 m^2/g.

One can then compare the low specific surface area of SWy-3 montmorillonite to that of K10 and KSF montmorillonites due to the fact that SWy-3 contains much more sodium (Na) in its structure (For K10, the weight percentage of Na2O is less than 0.3 %, whereas for SWy-3 it is around 1.6 %). On the other hand, the treatment of montmorillonite with sulfuric acid results in the replacement of the clay's structural cations (Al^{3+}, Mg^{2+}, Fe^{3+}) by protons (H^+), which leads to a substantial increase in the surface acidity of the clay. This phenomenon appears to be the cause of the better adsorption capacity of K10 montmorillonite compared to KSF and SWy-3.

As can be seen in Fig. 3.b, the pore size distribution follows a Gaussian shape, and the pore diameter appears to be relatively similar between the three montmorillonites, with values of 3.90, 3.94, and 3.71 nm for K10, KSF, and SWy-3, respectively.

In conclusion, the sulfuric acid treatment used to prepare the K10 and KSF montmorillonites at different concentrations shows, based on the specific surface area measured by BET, that adsorption on the clay surface is three times greater for K10 than for KSF (280 m^2/g for K10 compared to approximately 98 m^2/g for KSF) and six times greater for K10 compared to SWy-3 (280 m^2/g for K10 compared to 45 m^2/g). Finally, adsorption is two times greater for KSF than for SWy-3 (97 m^2/g for KSF compared to 45 m^2/g for SWy-3). It also seems that the anionic nature of SWy-3 montmorillonite, along with its high sodium (Na) content, hinders adsorption on its surface.

3.1.2. Cases of K10, KSF, and SWy-3 MMTs modified by the $[M(CH_2)IM^{2+}][2I^-]$ dicationic ionic liquid

The nitrogen adsorption-desorption isotherms of K10, KSF, and SWy-3 montmorillonites modified by the dicationic liquid $[M(CH_2)IM^{2+}][2I^-]$ are presented in Fig. 4a. In Fig. 4a, the adsorption-desorption isotherms are classified as type I*V* according to the IUPAC classification. Table 3 presents the different BET parameters: the BET surface area (S_{BET}) in m^2/g, the pore volume (V_{pores}) in cm^3/g, and the pore diameter (d_{pores}) calculated from the desorption isotherm.

From Table 3 and Fig. 4a and b, a significant decrease in the specific surface area (SBET) is observed after the addition of dicationic ionic liquids to the K10 clay: the surface area drops from 280 m^2/g for pure K10 to approximately 91 m^2/g for K10 + $[M(CH_2)IM^{2+}][2I^-]$. At the same time, the pore volume decreases considerably with the introduction of ionic liquids into the clay. Between pure K10 and K10 + $[M(CH_2)IM^{2+}][2I^-]$, the pore volume is reduced by a factor of 2.5. This decrease is evidently related to the amount of ionic liquid, suggesting that the liquid is occupying the pores. The reduction in both specific surface area and pore volume indicates that the ionic liquids are located within the interstitial volume of K10 montmorillonite.

Furthermore, a decrease in pore diameter is also observed (see Table 3), from 3.9 nm to 3.5 nm upon introducing the dicationic ionic liquid with the I^- anion. Additionally, a broadening of the pore diameter distribution is noted (see Fig. 4b), ranging from 3 to 10 nm. This phenomenon is correlated with the sudden release of gaseous nitrogen in the desorption curve, which is more pronounced at $P/P_o = 0.45$ for K10 + $[M(CH_2)IM^{2+}][2I^-]$. This suggests that most of the interparticle pore spaces are occupied by the ionic liquid.

From Table 3 and Fig. 4a and b, it can be observed that the specific surface area (S_{BET}), pore volume, and pore diameter after the addition of the dicationic ionic liquid with the I^- anion to the KSF clay are almost identical to those obtained for pure KSF. The intercalation of this ionic liquid into the interlayer space of KSF montmorillonite appears to slightly inhibit the passage of nitrogen molecules.

Thus, for KSF+$[M(CH_2)IM^{2+}][2I^-]$, the ionic liquid molecules are

Table 3
Results obtained by the BET method on purified K10, KSF, and SWy-3 MMTs modified by the *$[M(CH_2)IM^{2+}][2I^-]$* dicationic ionic liquid. (S_{BET} = BET specific surface area and V = Pore volumes).

Clays	S_{BET} (m^2/g)	V_{pores} (cm^3/g)	d_{pores}(nm)
K10	91 ± 1	0.06 ± 0.01	3.55 ± 0.02
KSF	91 ± 1	0.12 ± 0.01	3.91 ± 0.02
SWy-3	3 ± 1	0.03 ± 0.01	7.10 ± 0.02

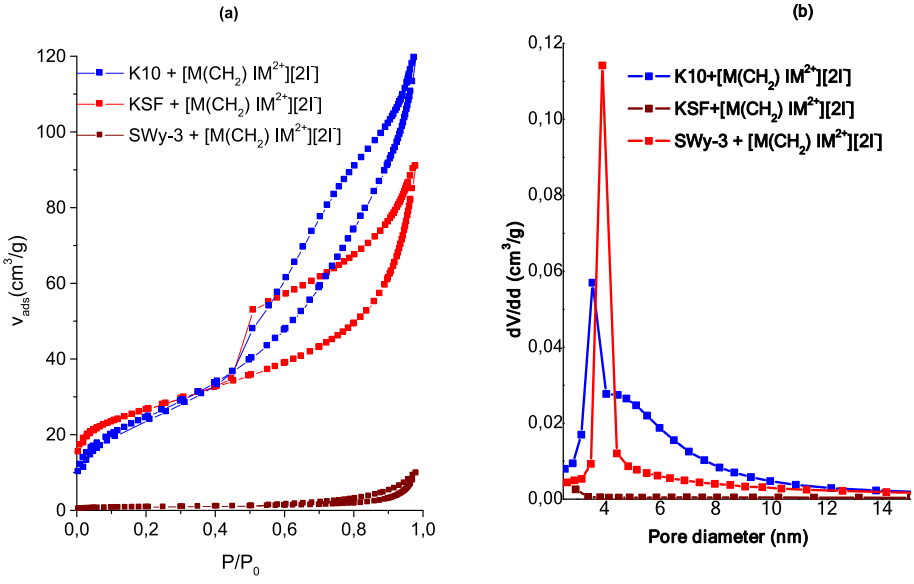

Fig. 4. Adsorption–desorption isotherms for K10, KSF, and SWy-3 MMTs modified by the $[M(CH_2)IM^{2+}][2I^-]$ dicationic ionic liquid (a) and pore size distribution for K10, KSF, and SWy-3 MMTs modified by the $[M(CH_2)IM^{2+}][2I^-]$ dicationic ionic liquid (b).

almost exclusively located in the interstitial space, as no increase in the pore diameter distribution is observed (see Fig. 4b), and there is a noticeable sudden release of gaseous nitrogen in the desorption curve at $P/P_o = 0.45$ (see Fig. 4a).

For SWy-3, the specific surface area (SBET) drops significantly with the addition of the dicationic ionic liquid, decreasing from 45 m^2/g to 3 m^2/g. Additionally, there is an expansion in pore diameter, increasing from 3.71 nm to 7.10 nm.

Thus, we observe that the impact of adding the dicationic ionic liquid $[M(CH_2)IM^{2+}][2I^-]$ on the BET parameters is much more significant for SWy-3 than for K10 and almost negligible for KSF.

3.2. Comparison between HTS/FTIR spectra of K10, KSF, and SWy-3 MMTs

The HTS/FTIR spectra (4000–600 cm^{-1}) of the three purified montmorillonites (K10, KSF, and SWy-3) are shown in Fig. 5. All spectra are normalized to the mode at 1240 cm^{-1}. The assignments of the observed modes in this spectral region are listed in Table 4.

In the HTS spectra (see Fig. 5), three distinct spectral regions 3800–2600 cm^{-1}, 2000–1500 cm^{-1}, and 1500–1000 cm^{-1} can be clearly distinguished. These spectral regions are displayed in Fig. 5a–c, respectively. For the three different montmorillonites, all samples exhibited similar vibrational behavior, with slight variations in band positions (Table 3) and in the intensity of several peaks (Tables 4 and 5).

3.2.1. Region 3800–2600 cm^{-1} (O—H stretching region)

The HTS/FTIR spectra in this spectral region (Fig. 6a) did not reveal significant vibrational differences between the three clays. All spectra were normalized to the mode at 3635 cm^{-1}. Four peaks, more or less defined, were observed at 3695 cm^{-1} and 3630 cm^{-1}, assigned to O—H stretching of inner hydroxyl groups coordinated to octahedral cations, and at 3425 cm^{-1} with a shoulder near 3235 cm^{-1}, corresponding to O—H stretching of water [24–26].

Small differences in peak intensity were also observed among the three montmorillonite clays. Table 5 presents the intensity ratios between the observed components, defined as I_{3405}/I_{3635} = I(ν(O–H) of water)/I(ν(O–H) related to cations) and I_{3225}/I_{3635} = I(ν(O–H) of water)/I(ν(O–H) related to cations) for the different samples.

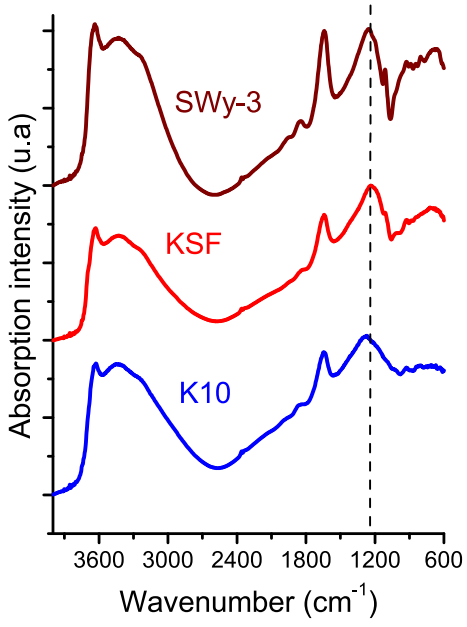

Fig. 5. HTS/FTIR spectra of purified K10, KSF, and SWy-3 montmorillonites in the spectral ranges 4000–600 cm^{-1}. The black dashed line represents the mode at 1240 cm^{-1}, which was taken as the reference for spectrum normalization.

Table 4
HTS/FTIR assignments of K10, KSF and SWy-3 montmorillonites (w = weak; *vw* = very weak; m = medium; s = strong; vs = very strong; * = value of fit; (sh) = shoulder; n = str = stretching; δ = deformation: ip = in the plane); *** = not measured [8,20,21,22,23].

K10	KSF	SWy-3	Assignment
4000–2500 cm^{-1}			
3697*(sh)	3699* (sh)	3399* (sh)	*ν*(OH) of inner-surface hydroxyl groups
3630 (m)	3629 (m)	3635 (m)	*ν*(OH) of structural OH groups
3425 (m)	3430 (m)	3427 (m)	*ν*(OH) of water
3244*(sh)	3240* (sh)	3235* (sh)	*ν*(OH) of water
2000–1000 cm^{-1}			
1970*(sh)	1938* (sh)	1960* (sh)	Water libration
1858 (m)			Water libration
1633 (s)	1845 (m) 1633 (m)	1850 (m) 1628 (m)	δ (OH) of water
1423*(sh)	1412* (sh)	1440* (sh)	δ (O—H) ip vibration
***	1371 (sh)	1326 (sh)	δ (O—H) ip vibration
1290 (vs)	1240 (vs)	1242 (vs)	δ (O—H) ip vibration
1169*(sh)	1169* (sh)	1194* (sh)	*ν*(Si—O)
***	***	1103* (sh)	*ν*(Si—O)
1071*(sh)	1106 (m)	1108 (m)	*ν*(Si—O)
1019*(sh)	1008 (m)	1019* (sh)	*ν*(Si—O)

Table 5
Intensity ratios of various peaks of purified K10, KSF, and SWy-3 MMTs in the spectral range 4000–3000 cm^{-1}.

Clays	I_{3400}/I_{3635}	I_{3225}/I_{3635}	I_{3400}/I_{3225}
K10	1.00 ± 0.02	0.86 ± 0.02	1.16 ± 0.02
KSF	0.92 ± 0.02	0.78 ± 0.02	1.18 ± 0.02
SWy-3	0.81 ± 0.02	0.69 ± 0.02	1.17 ± 0.02

From this table, we note a significant variation in intensity ratios among K10, KSF, and SWy-3. Specifically, the ratios I_{3405}/I_{3635} and I_{3225}/I_{3635} decrease by 20 % from K10 to SWy-3, suggesting that the higher Na^+ ion content in SWy-3 significantly influences the distribution of water molecules within the clay sheet structure. However, the ratio I_{3405}/I_{3225} = I(ν(O–H) of water)/I(ν(O–H) of water) remained similar for K10, KSF, and SWy-3.

3.2.2. Region 2000–1000 cm^{-1}

In Fig. 6b and c, the HTS/FTIR results for K10, KSF, and SWy-3 in the spectral range of 2000–1000 cm^{-1} are presented. All spectra are normalized to the mode at 1250 cm^{-1}.

In the spectral region 2000–1800 cm^{-1}, intense modes assigned to water libration [25] are observed, more or less defined at 1960 and 1850 cm^{-1} [22]. These two peaks result from water libration, with some water molecules remaining on the clay surface, while others are located deeper within the clay structure.

In the spectral region 1700–1200 cm^{-1}, intense modes assigned to the O—H bending deformation of water molecules [27,20] are observed, more or less defined at 1635, 1440, and 1250 cm^{-1}. Additionally, in the spectral region 1200–1000 cm^{-1}, three peaks appear at 1194, 1110, and 1019 cm^{-1}, which are more pronounced in SWy-3 and KSF than in K10 and are assigned to the Si—O stretching mode [24,25,27].

We note that the most intense peak near 1250 cm^{-1} varies in frequency among the three clays: 1290 cm^{-1} for K10, 1240 cm^{-1} for KSF, and 1242 cm^{-1} for SWy-3, corresponding to a variation of approximately 40 cm^{-1}. This suggests that Na^+ plays a significant role in the

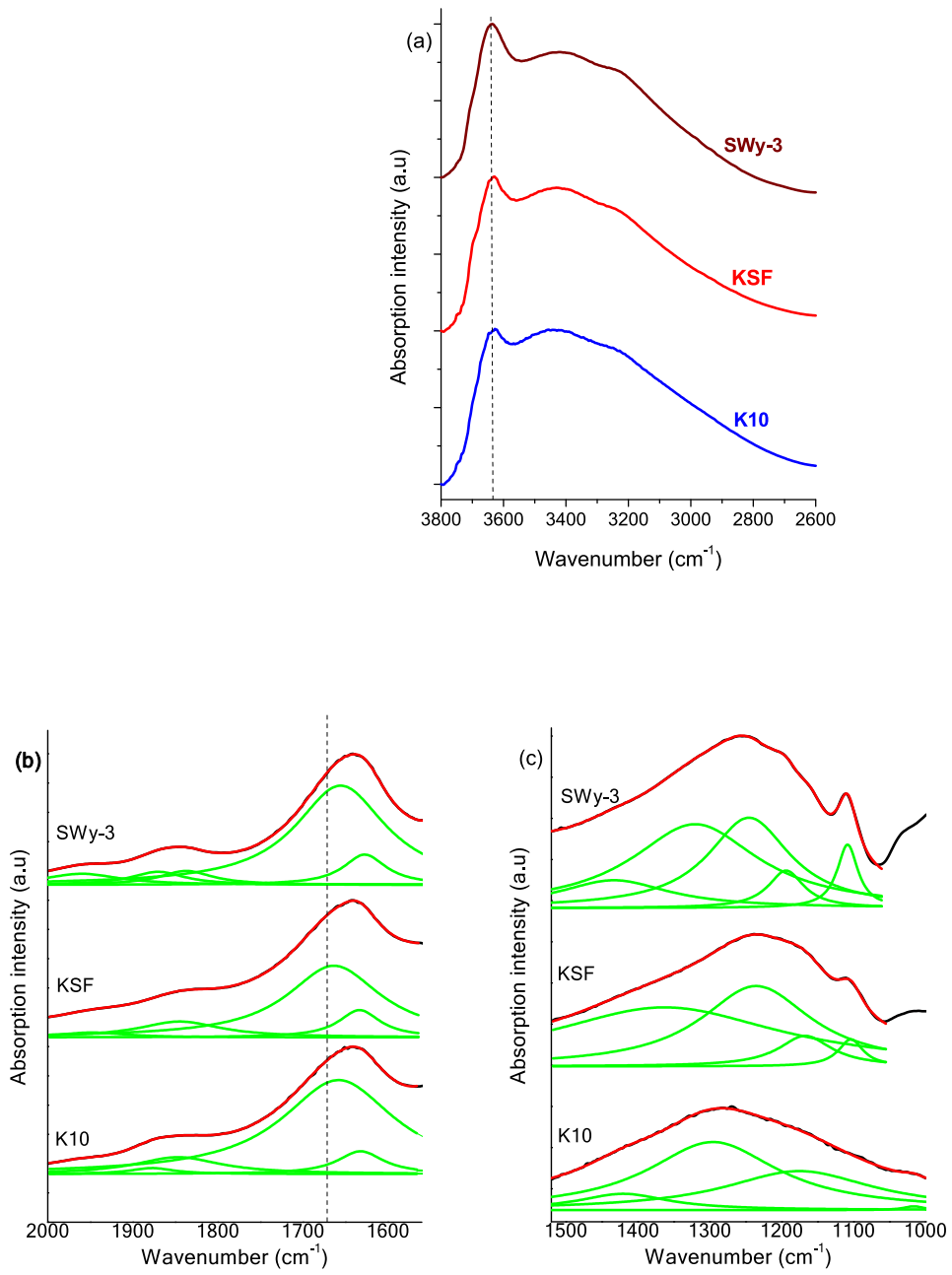

Fig. 6. HTS/FTIR spectra of purified K10, KSF, and SWy-3 montmorillonites in the following spectral ranges: (a) 3800–2600 cm^{-1} (the black dashed line indicates the mode at 3635 cm^{-1}), and fitted with Lorentzian curves in two spectral regions: (b) 2000–1550 cm^{-1} (the black dashed line indicates the mode at 1633 cm^{-1}) and (c) 1500–1000 cm^{-1}. The black line represents the measured spectrum, the green lines correspond to the different Lorentzian functions used to fit the selected spectral regions, and the red curve is the reconstructed spectrum obtained from the convolution of the green lines. (For interpretation of the references to colour in this figure legend, the reader is referred to the web version of this article.)

clay structure. Indeed, Na^+ ions in SWy-3 MMT occupy cation exchange sites in the montmorillonite structure, replacing other cations present in K10 or KSF, such as Ca^{2+}, Mg^{2+}, or K^+. Since Na^+ is a monovalent ion, it facilitates cation exchange with other substances, which is particularly important for applications such as pollutant adsorption and water purification.

Table 6 presents the intensity ratios:

- $\eta_1 = I_{1850}/I_{1633}$ = I(water libration)/I(δ(O − H) of water
- $\eta_2 = I_{1633}/I_{1250}$ = I(δ(O − H) of water)/I(δ(O − H) of water in the plane
- $\eta_3 = I_{1110}/I_{1250}$ = I(ν(Si − O))/I(δ(O − H) of water in the plane

Table 6
Intensity ratios of various peaks of purified K10, KSF, and SWy-3 MMTs in the spectral range 2000–1000 cm^{-1}.

Clays	I_{1850}/I_{1633}	I_{1633}/I_{1250}	I_{1110}/I_{1250}
K10	0.24 ± 0.02	0.83 ± 0.02	0.74 ± 0.02
KSF	0.22 ± 0.02	0.71 ± 0.02	0.72 ± 0.02
SWy-3	0.20 ± 0.02	0.97 ± 0.02	0.65 ± 0.02

From these data, notable differences in the intensity ratios η_2 and η_3 are observed for K10, KSF, and SWy-3. These differences indicate that the distribution of water molecules in the three clays is not identical, likely due to the presence of Na^+ or differences in their structures. In

particular, the intensity ratio $\eta_2 = I_{1633}/I_{1250}$ varies significantly: its value is 0.71 for KSF MMT, which is 15 % lower than for K10 MMT and 26 % lower than for SWy-3.

3.3. Comparison of HTS/FTIR spectra for clays modified with I^- anion

3.3.1. Case of monocationic ionic liquid

The HTS/FTIR spectra (4000–600 cm^{-1}) of K10, KSF, and SWy-3 modified by [$EMIM^+$][I^-] are presented in Fig. 7. The spectrum is normalized to the mode at 1230 cm^{-1}. The assignments of the observed modes are listed in Table 7.

In the HTS spectra (see Fig. 7), two well-defined spectral regions can be distinguished: 3800–2600 cm^{-1} and 2000–1000 cm^{-1}. These spectral regions are illustrated in Figs. 8 and 9, respectively.

In the spectral ranges 3200–2800 cm^{-1} and 1800–1000 cm^{-1}, the appearance of new peaks is observed, primarily corresponding to the signature modes indicating the presence of [$EMIM^+$][I^-] in the three montmorillonites.

3.3.1.1. The spectral region 3800–2600 cm^{-1}. In this spectral region (Fig. 8), all spectra are normalized to the peak at 3625 cm^{-1}. This region can be divided into two zones (see Fig. 8): 3800–3200 cm^{-1} and 3200–2800 cm^{-1}. To better understand the spectral differences observed in the IR spectra of the modified clays, Fig. 10a and b present the ATR/FTIR spectra of the ionic liquids used.

The first zone corresponds to vibrational modes attributed to the O—H stretching of water, which are influenced by the presence of [$EMIM^+$][I^-] within the montmorillonite structure. By comparing the results obtained for clays modified with [$EMIM^+$][I^-] (Table 8) with those of unmodified clays (Table 5), we observe two main phenomena.

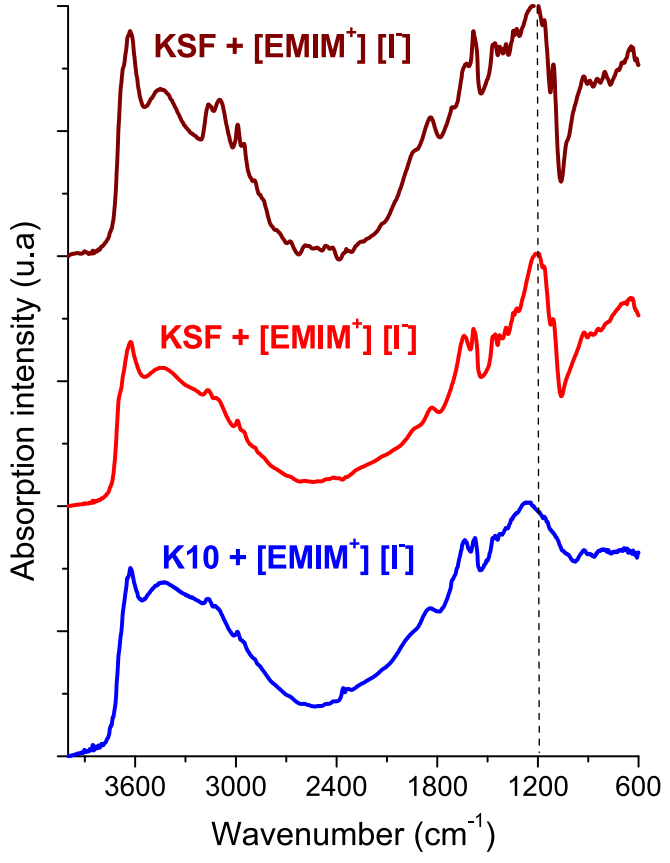

Fig. 7. HTS/FTIR spectra of K10, KSF, and SWy-3 modified by [$EMIM^+$][I^-] in the spectral range of 4000–600 cm^{-1}. The black dashed line indicates the mode at 1200 cm^{-1}, which was used as the reference for spectrum normalization.

Table 7
HTS/FTIR assignments of K10, KSF, and SWy-3 modified by [$EMIM^+$] [I^-]. (w = weak; vw = very weak; m = medium; s = strong; vs = very strong; * = value of fit; (sh) = shoulder; n = str = stretching; δ = deformation; ip = in the plane; as = asymmetric); *** = not measured. [8,20,21,22,28,29].

K10 + [EMIM+] [I−]	KSF + [EMIM+] [I−]	SWy-3 + [EMIM+] [I−]	Assignment
		3800–2600 cm^{-1}	
3629 (m)	3627 (m)	3629 (m)	ν(OH) vibrations
3423 (m)	3435 (m)	3450 (m)	ν (OH) of water
3250*(sh)	3248*(sh)	3259*(sh)	ν (OH) of water and ν(N—H)
3162 (m)	3167 (m)	3163 (m)	ν(N—H) and ν(C—H)
3106 (m)	3102 (m)	3097 (m)	ν(N—H) and ν(=C-H)
2991 (w)	2989 (w)	2989 (m)	ν(N—H) and ν(C—H)
2949 (w)	2949 (w)	2949 (m)	ν(N—H) and ν(C—H)
		2000-1000 cm^{-1}	
1980*(sh)	***	1945*(sh)	Water libration
1854 (w)	1834 (w)	1839 (w)	Water libration
1707 (w)	1712*(sh)	1714 (w)	Overtone ν(C=C-H)
1639 (s)	1646 (m)	1651 + 1621 (s)	Ring ν(C=C), ν(N=C-N) and δ(OH)
1573 (s)	1574 (m)	1583 + 1565 (s)	$\nu_{as}(CH_2(N))$, $\nu(CH_3(N)CN$
1470 (s)	1469 (s)	1469 (s)	$\delta(CH_2)$, $\delta_{as}(CCH)$, $\delta_{as}(HCH)$
1455 (s)	1454 (m)	1455 (s)	$\delta(CH_2)$, $\delta_{as}(CCH)$, $\delta_{as}(HCH)$
1421 (s)	1429 (m)	1429 (s)	δ(O—H), $CH_2(N)$, $CH_3(N)CN$ Str
1390 (s)	1388 (m)	1390 (s)	$CH_2(N)$, $CH_3(N)CN$ Str
1346 (s)	1346 (s)	1346 (s)	$CH_2(N)$, $CH_3(N)$ CN str
1327 (s)	1322 (s)	1327 (m)	$CH_2(N)$, $CH_3(N)$ CN str
1250 (vs)	1201 (vs)	1211 (vs)	δ(C—H) and δ(O—H) ip vibration
1163 (s)	1163 (s)	1161 (vs)	ν(Si—O),$\nu_{as}(CH_2(N))$, ν $(CH_3(N)CN$
1085*(sh)	1111 (s)	1107 (s)	ν(Si—O), ν(C—C)

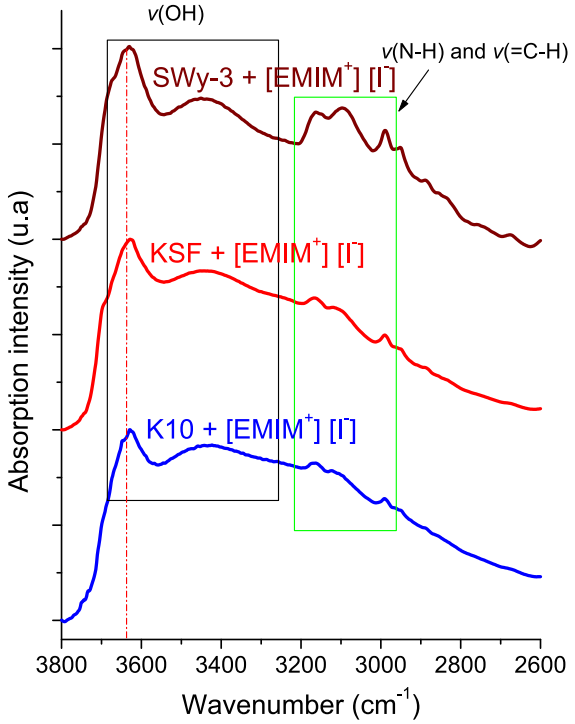

Fig. 8. HTS/FTIR spectra of K10, KSF, and SWy-3 modified by [$EMIM^+$][I^-] in the spectral range of 3800–2600 cm^{-1}. The black dashed line indicates the mode at 3635 cm^{-1}.

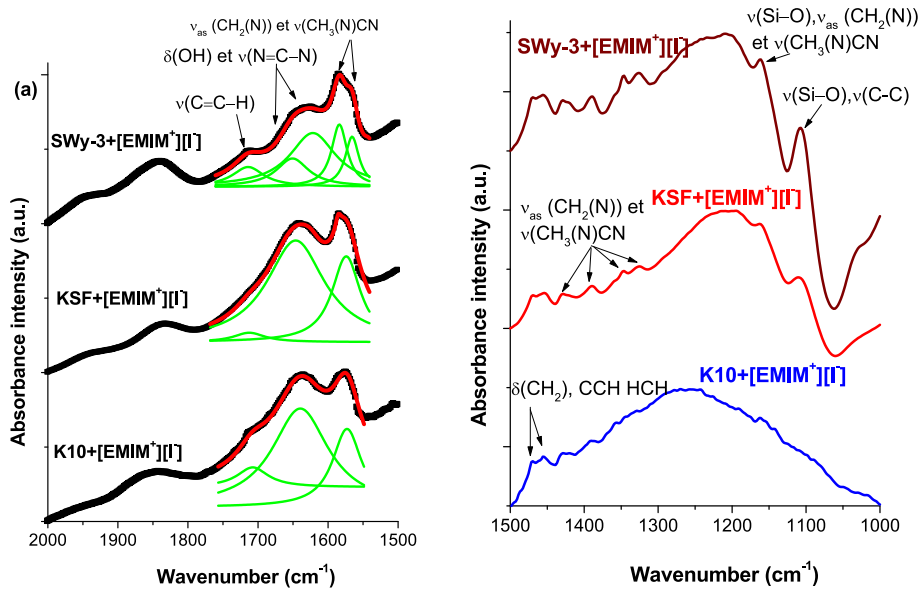

Fig. 9. HTS/FTIR spectra of K10, KSF, and SWy-3 modified by [$EMIM^+$][I^-] in the spectral ranges (a) 2000–1500 cm^{-1} and (b) 1500–1000 cm^{-1}. The green curves represent the fitting of the existing vibrational modes in these spectral regions using Lorentzian functions. The red curve represents the overall fit, which closely matches the experimental curve shown in black. (For interpretation of the references to colour in this figure legend, the reader is referred to the web version of this article.)

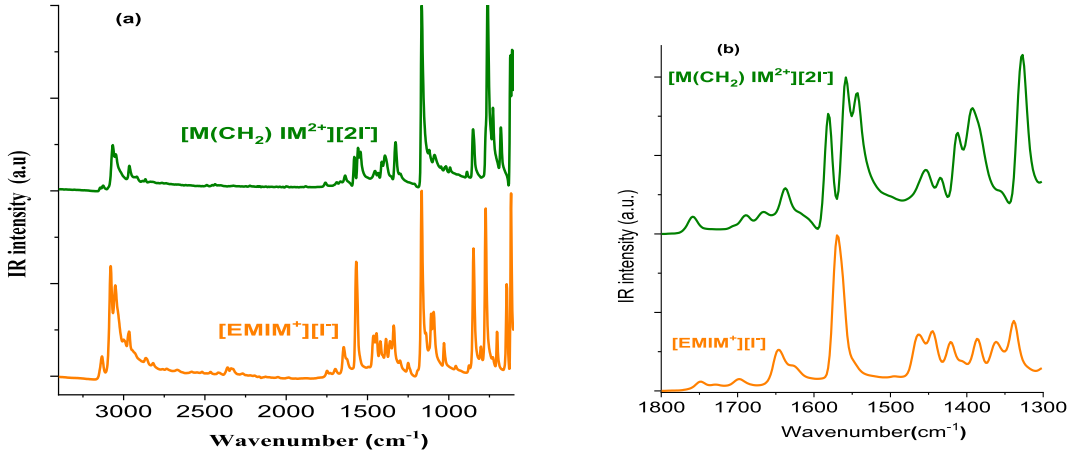

Fig. 10. ATR/FTIR spectra of [$EMIM^+$][I^-] and [$M(CH_2)IM^{2+}$][$2I^-$] in the spectral regions (a) 3400–600 cm^{-1} and (b) 1800–1300 cm^{-1}.

Table 8
Intensity ratios of various peaks for K10, KSF, and SWy-3 modified by the [$EMIM^+$][I^-] ionic liquid in the spectral range 3800–2600 cm^{-1}.

Modified Clays	I_{3400}/I_{3635} [$EMIM^+$] [I^-]	I_{3160}/I_{3115} [$EMIM^+$] [I^-]
K10	0.93 ± 0.02	1.07 ± 0.02
KSF	0.84 ± 0.02	1.09 ± 0.02
SWy-3	0.75 ± 0.02	0.96 ± 0.02

First, significant shifts occur in the mode assigned to the ν(O—H) stretching of water at 3400 and 3225 cm^{-1} [10,18,26]. Specifically, for K10 modified with [$EMIM^+$][I^-], shifts of approximately +5 and − 5 cm^{-1} are observed for the peaks at 3400 and 3225 cm^{-1}, respectively. For KSF, the shifts are +5 and + 10 cm^{-1}, while for SWy-3, both peaks shift by +15 cm^{-1}.

Second, a notable increase in intensity is observed for the ν(O—H) stretching mode of water. To quantify these changes, Table 6 presents the intensity ratio of the two peaks at 3635 and 3400 cm^{-1} for the three clays modified with [$EMIM^+$][I^-]. This ratio is defined as $\mu_1 = I_{3400}/I_{3635}$ = I(ν(O—H) of water)/I(ν(O—H)). In comparison with the same intensity ratio calculated for purified montmorillonite (see Table 5), μ_1 decreases from 1.00 to 0.93 for K10, from 0.92 to 0.84 for KSF, and from 0.82 to 0.75 for SWy-3.

These two phenomena demonstrate that the presence of the ionic liquid within the structure of the three clays has a direct and significant impact, affecting the vibrational modes associated with ν(O—H) stretching in different ways.

In the second zone, dominated by N—H and C—H vibrations [9,18,30], we observe the peaks at 3133, 3052, and 2995 cm^{-1} for [$EMIM^+$][I^-], which shift to 3162, 3106, and 2990 cm^{-1} (approximately +30, +55, −5 cm^{-1}), respectively, for K10 modified by [$EMIM^+$][I^-]. For KSF modified by [$EMIM^+$][I^-], the shifts are around +35, +50, and − 5 cm^{-1}. For SWy-3 modified by [$EMIM^+$][I^-], the shifts are approximately +30, +45, and − 5 cm^{-1}.

We also note that the peak at 2967 cm^{-1}, associated with ν(CH_2HCH) for [$EMIM^+$][I^-] [9,18], shifts to 2950 cm^{-1} (−15 cm^{-1}) for all three clays. As with the previous analysis (see Table 4), we can estimate a new

intensity ratio between the three modified clays, defined as $\mu_2 = I_{3160}/I_{3115} = I(\nu(N—H))/I(\nu(N—H), \nu(C—H))$, with values of 1.07 for K10, 1.09 for KSF, and 0.96 for SWy-3. This confirms that K10 and KSF modified clays exhibit similar behavior in this region.

3.3.1.2. The spectral Region 2000–1000 cm^{-1}. We divide this region into two zones: the 2000–1500 cm^{-1} zone, shown in Fig. 9a, and the 1500–1000 cm^{-1} zone, shown in Fig. 9b. In the first zone, we observe peaks at 1698 cm^{-1}, assigned to the stretching modes of C═C and N═C-N bonds [21], and at 1569 cm^{-1}, assigned to the stretching modes of $CH_2(N)$ and $CH_3(N)CN$ [18,21,22] for [EMIM$^+$][I$^-$]. These peaks are shifted by approximately +10 and + 5 cm^{-1}, respectively, for K10 modified by [EMIM$^+$][I$^-$]. For KSF modified by [EMIM$^+$][I$^-$], the shifts are around +15 and + 5 cm^{-1}. However, for modified SWy-3, the 1698 cm^{-1} peak shifts by approximately +15 cm^{-1}, while the 1569 cm^{-1} peak splits into two peaks at 1583 and 1565 cm^{-1}.

We also observe the peak at 1633 cm^{-1}, assigned to the bending mode of O—H in water molecules for unmodified clay, shifted to 1639 cm^{-1} for K10 and 1646 cm^{-1} for KSF. However, for modified SWy-3, the 1633 cm^{-1} peak splits into two peaks at 1651 and 1665 cm^{-1}.

By comparing the intensity ratios for purified clays (Table 6) with those calculated for clays modified by [EMIM$^+$][I$^-$] (Table 9), we observe different intensity ratios between the three modified clays, defined as:

- $k_1 = I_{1850}/I_{1633} = I(\delta(O—H))/I[\delta(O—H)$ water, $\nu(C=C)$, $\nu(N=C-N)]$,
- $k_2 = I_{1633}/I_{1250} = I[\delta(O—H)$ water, $\nu(C=C)$, $\nu(N=C-N)]/I[\delta(O—H)$ water, $\delta(C—H)]$,
- $k_3 = I_{1105}/I_{1250} = I[\nu(Si—O)$, $\nu(C—C)]/I[\delta(O—H)$ water, $\delta(C—H)]$.

We note that k_1 for each modified clay differs from the value for purified MMT. This demonstrates that the presence of [EMIM$^+$][I$^-$] inside the three clays has a different effect on the ν(O—H) mode of water in each clay. For k_1: K10 increases from 0.24 to 0.93, KSF from 0.22 to 0.32, and SWy-3 from 0.20 to 0.46. For k_2: K10 decreases from 0.83 to 0.27, KSF from 0.71 to 0.56, and SWy-3 from 0.97 to 0.62.

In the second zone, we observe the presence of new peaks attributed solely to [EMIM$^+$][I$^-$] around 1463 cm^{-1}, corresponding to $\delta(CH_2)$, ν(CCH HCH) [9,21], and 1421 cm^{-1}, corresponding to $\nu(CH_2(N))$, $\nu(CH_3(N))$ [20]. The first peak shifts by approximately −10 cm^{-1} for all three clays, but the second peak appears at 1421 cm^{-1} for modified K10, while for KSF and SWy-3, it shifts by approximately +10 cm^{-1}.

We also observe three new peaks at 1386, 1361, and 1338 cm^{-1}, corresponding to $\nu(CH_2(N))$, $\nu(CH_3(N))$ [16]. The 1386 cm^{-1} peak shifts by approximately +5 cm^{-1} for modified K10 and SWy-3. However, the 1361 cm^{-1} peak shifts by approximately −15 cm^{-1} for all three modified clays. The 1338 cm^{-1} peak shifts by approximately −10 cm^{-1} for K10 and SWy-3, and by −5 cm^{-1} for KSF.

We also observe significant shifts for two modes assigned to the stretching vibrations of ν(O—H) and Si-O: 1250 and 1110 cm^{-1}. The first shifts by approximately −20, −25, and + 5 cm^{-1} for K10, KSF, and SWy-3 modified with [EMIM$^+$][I$^-$], respectively. The changes in wavenumber for the peak at 1110 cm^{-1} are less significant, with shifts of approximately +15 and + 5 cm^{-1} for K10 and KSF modified with [EMIM$^+$][I$^-$], respectively.

Table 9
Intensity ratios of various peaks of K10, KSF, and SWy-3 modified by the ionic liquid [EMIM$^+$][I$^-$] in the spectral domain 2000–1000 cm^{-1}.

Modified Clays	I_{1850}/I_{1633} [EMIM$^+$] [I$^-$]	I_{1633}/I_{1250} [EMIM$^+$] [I$^-$]	I_{1105}/I_{1250} [EMIM$^+$] [I$^-$]
K10	0.93 ± 0.02	0.27 ± 0.02	0.78 ± 0.02
KSF	0.32 ± 0.02	0.56 ± 0.02	0.65 ± 0.02
SWy-3	0.46 ± 0.02	0.62 ± 0.02	0.62 ± 0.02

3.3.2. Case of dicationic ionic liquid

The HTS/FTIR spectra in the 4000–600 cm^{-1} range of the three montmorillonites (MMTs) modified with [M(CH$_2$)IM^{2+}][2I$^-$] are shown in Fig. 11. Each spectrum has been normalized to the mode at 1220 cm^{-1}. The assignments of the observed modes in this spectral region are reported in Table 10. In the HTS spectra (see Fig. 11), two well-defined spectral regions can be distinguished: 3800–2500 cm^{-1} and 2000–1000 cm^{-1}. These two spectral regions are illustrated in Figs. 12 and 13, respectively. The latter region is further divided into two well-defined spectral ranges: 2000–1500 cm^{-1} and 1500–1000 cm^{-1}, as shown in Fig. 13a and b, respectively.

3.3.2.1. The spectral Region 3800–2600 cm^{-1}. In this spectral region (Fig. 10), all spectra are normalized to the peak at 3635 cm^{-1}. This region is divided into two zones (see Fig. 10): the zone from 3800 to 3200 cm^{-1} and the zone from 3200 to 2800 cm^{-1}. In the first zone, we do not observe any significant vibrational differences between the purified clays and the clays modified with [M(CH$_2$)IM^{2+}][2I$^-$]. The only phenomenon that can be noted by comparing the results obtained from the clays modified with [M(CH$_2$)IM^{2+}][2I$^-$] (Table 7) with those for the purified clays (Table 2) is a significant shift in the mode attributed to the ν(O—H) of water for the peaks at 3400 and 3225 cm^{-1} [16,24,26,21]. These two peaks shifted by approximately +10 and + 15 cm^{-1}, respectively, for K10 modified with [M(CH$_2$)IM^{2+}][2I$^-$]. For KSF, the 3225 cm^{-1} peak shifts by approximately −10 cm^{-1}.

Table 11 shows that there is no notable change in the intensity of the mode attributed to ν(O—H) of water at 3625 and 3420 cm^{-1}. This table presents an intensity ratio between the three clays modified with [M(CH$_2$)IM^{2+}][2I$^-$], defined as: $\mu_1 = I_{3400}/I_{3635} = I(\nu$(O—H) of water)/I($\nu$(O—H)). In comparison with the same intensity ratio calculated for purified montmorillonite (see Table 3), μ_1 for K10 decreases from 1.00 to 0.97, for KSF from 0.92 to 0.90, and for SWy-3 from 0.82 to 0.84.

We observe that the introduction of [M(CH$_2$)IM^{2+}][2I$^-$] into the clay caused the appearance of new peaks: the 3144 cm^{-1} peak, attributed to

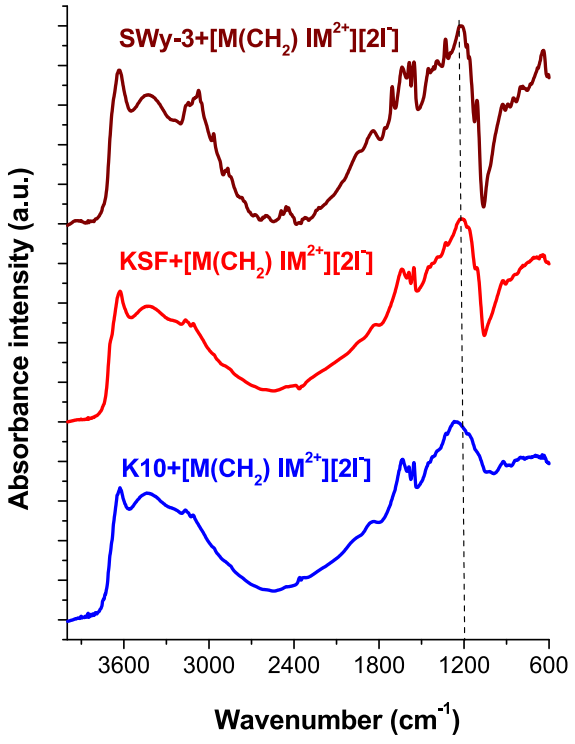

Fig. 11. The HTS/FTIR spectra of K10, KSF, and SWy-3 modified with [M(CH$_2$)IM^{2+}][2I$^-$] in the spectral range 4000–600 cm^{-1}. The black dashed line represents the mode at 1200 cm^{-1}.

Table 10
HTS/IFTR assignments of K10, KSF, and SWy-3 MMTs modified by [M(CH₂)IM^{2+}] [2I^{-}]. w = weak; vw = very weak; m = medium; s = strong; vs = very strong; * = value of fit; (sh) = shoulder; n = str = stretching; δ = deformation; ip = in the plane; as = asymmetric), *** = not measured. [8,20,21,22,28,29].

K10 + [M(CH₂)IM^{2+}] [2I^{-}]	KSF + [M(CH₂)IM^{2+}] [2I^{-}]	SWy-3 + [M(CH₂)IM^{2+}] [2I^{-}]	Assignment
		3800–2600 cm^{-1}	
3627 (m)	3627 (m)	3635 (s)	*ν*(OH) vibrations
3435 (m)	3428 (m)	3425(m)	*ν*(OH) of water
3242*(sh)	3232*(sh)	3235*(sh)	*ν*(OH) of water and *ν*(N—H)
3167 (m)	3165 (m)	3163*(sh)	*ν*(N—H) and *ν*(C—H)
3143*(sh)	3143*(sh)	3145 (m)	*ν*(N—H) and *ν*(C—H)
3113 (m)	3111 (m)	3106 (m)	*ν*(N—H) and *ν*(=C-H)
***	***	3073(m) + 3050*(sh)	*ν*(N—H) and *ν*(C—H)
2965*(sh)	2965*(sh)	2966 (m)	*ν*(CH₃)(N)HCH)
***	***	2883 (w) + 2868 (w)	*ν*(CH₂)
		2000-1000 cm^{-1}	
1847 (w)	1854 (w)	1841 (w)	Water libration
1699*(sh)	1704*(sh)	1756 + 1707 (w)	δ(OH), overtone *ν*(C=C-H)
1635 (s)	1637 (s)	1637 (s)	Ring *ν*(C=C), *ν*(N=C-N) and δ(OH)
1587 (s)	1587(s)	1585 (s)	ν_{as}(CH₂(N))/ *ν*(CH₃(N)CN
1567 (s)	1568 (s)	1564 (s)	*ν*(CH₂(N))/ *ν*(CH₃(N)CN
1552 (s)	1552 (s)	1550 (s)	*ν*(N=C)
1469*(sh)	1447*(sh)	1469*(sh)	δ(CH₂), δ_{as}(CCH), δ_{as}(HCH)
1452 (s)	1450 (s)	1452 (s)	δ(CH₂), δ_{as}(CCH), δ_{as}(HCH)
1425 (s)	1427 (m)	1427 + 1416 (s)	δ(O—H), CH₂(N), CH₃(N)CN Str
1390 (s)	1387 (m)	1390 (s)	CH₂(N), CH₃(N)CN Str
1327 (s)	1327 (s)	1330 (m)	CH₂(N), CH₃(N) CN str
1253 (vs)	1214 (vs)	1214 (vs)	δ(C—H) and δ (O—H) ip vibration
1168 (s)	1160 (s)	1176(s) + 1163 (vs)	*ν*(Si—O),ν_{as}(CH₂(N))/ *ν*(CH₃(N)CN
1093*(sh)	1109 (s)	1109 (s)	*ν*(Si—O), *ν*(C—C)

the stretching modes of C—H and N—H [27,28,29] for [M(CH₂)IM^{2+}] [2I^{-}], is transformed into two peaks at 3165 and 3144 cm^{-1} for the three modified clays. The 3126 cm^{-1} peak for [M(CH₂)IM^{2+}][2I^{-}] shifts to 3113, 3111, and 3106 cm^{-1} for K10, KSF, and SWy-3, respectively.

The peaks at 3066, 3049, 2883, and 2866 cm^{-1}, attributed to [M(CH₂)IM^{2+}][2I^{-}], shift only for modified SWy-3 to 3073, 3050, 2883, and 2868 cm^{-1}. It is possible to estimate a new intensity ratio between the three modified clays, defined by $\mu_2 = I_{3160}/I_{3115} = I(\nu(N—H))/I[\nu(N—H), \nu(=C-H)]$, with values of 1.05 for K10, 1.04 for KSF, and 0.97 for SWy-3. This confirms that K10 and KSF modified clays exhibit similar behavior in this region.

3.3.2.2. The spectral Region 2000–1000 cm^{-1}. We divide this region into two zones: the 2000–1500 cm^{-1} zone shown in Fig. 11.a and the 1500–1000 cm^{-1} zone shown in Fig. 11.b. In the first zone, we observe the peaks at 1698, 1581, 1558, and 1543 cm^{-1} assigned to [M(CH₂)IM^{2+}][2I^{-}], which shift approximately +1, +5, +10, and + 10 cm^{-1}, respectively, for K10 modified by [M(CH₂)IM^{2+}][2I^{-}]. For KSF modified by [M(CH₂)IM^{2+}][2I^{-}], the shifts are around +5, +5, +10, and + 10 cm^{-1}. For SWy-3 modified, the peak at 1698 cm^{-1} splits into two peaks: 1756 and 1707 cm^{-1}, but the 1581, 1558, and 1543 cm^{-1} peaks shift by approximately +5, +5, and + 5 cm^{-1}. We observe that the 1633 cm^{-1} peak, assigned to the O—H bending mode of water molecules [30] for

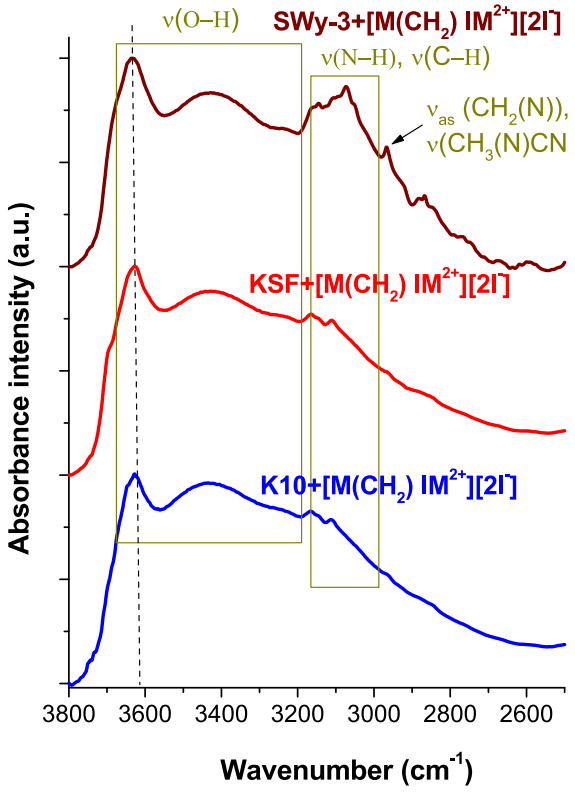

Fig. 12. The HTS/FTIR spectra of K10, KSF, and SWy-3 modified with [M(CH₂)IM^{2+}][2I^{-}] in the spectral range of 3800–2600 cm^{-1}. The black dashed line represents the mode at 3635 cm^{-1}.

unmodified clay, shifts by approximately +2, +5, and + 15 cm^{-1} for K10, KSF, and SWy-3, respectively, ascribed to O—H bending modes [30] and *ν*(N=C-N) [3,23].

In Table 12, we present the various intensity ratios among the three clays modified by [M(CH₂)IM^{2+}][2I^{-}], defined as:

$k_1 = I_{1850}/I1_{633} = I\delta(O—H)/I[\delta(O—H)$ of water, $\nu(C=C)$, $\nu(N=C-N)]$

$k_2 = I_{1633}/I_{1250} = I[\delta(O—H)$ of water, $\nu(C=C)$, $\nu(N=C-N)]/I[\delta(O—H)$ of water, $\delta(C—H)]$

$k_3 = I_{1105}/I_{1250} = I[\nu(Si—O)$, $\nu(C—C)]/I[\delta(O—H)$ of water, $\delta(C—H)]$.

By comparing Table 12 with Table 4, we observe that k_1 for each modified clay (K10, KSF, and SWy-3) differs from their values in purified K10, KSF, and SWy-3. This confirms that the introduction of [M(CH₂)IM^{2+}][2I^{-}] inside the three clays had a different effect on intensity in each clay. For k_1: K10 changes from 0.24 to 0.26, KSF from 0.22 to 0.31, and SWy-3 from 0.20 to 0.37. For k_2: K10 changes from 0.83 to 0.67, KSF from 0.71 to 0.61, and SWy-3 from 0.97 to 0.68. For k_3: K10 changes from 0.74 to 0.71, KSF from 0.72 to 0.62, and SWy-3 from 0.65 to 0.45. We note that, in all three cases, the intensity ratio was more significantly changed for SWy-3 by approximately (+46.0 %, −29.9 %, −30.8 %), while for K10 it changed by approximately (+7.7 %, −19.0 %, −4.1 %), and (+29.0 %, −14.0 %, −13.9 %) for KSF.

In the second zone, we observe the presence of new peaks attributed solely to [M(CH₂)IM^{2+}][2I^{-}] around 1454 and 1435 cm^{-1}, corresponding to δ(CH₂) and *ν*(CCH) [3]. The peak at 1454 cm^{-1} appears at 1452, 1450, and 1452 cm^{-1} for modified K10, KSF, and SWy-3, respectively. However, the peak at 1435 cm^{-1} shifts by approximately −10 cm^{-1} for modified K10 and KSF, while for modified SWy-3, it splits into two peaks at 1427 and 1416 cm^{-1}.

A similar pattern is observed for the two peaks at 1389 and 1350 cm^{-1}, which correspond to *ν*(CH₂(N)) and *ν*(CH₃(N)) [11], attributed solely to [M(CH₂)IM^{2+}][2I^{-}]. The peak at 1389 cm^{-1} appears at 1390, 1387, and 1390 cm^{-1} for modified K10, KSF, and SWy-3, respectively. The peak at 1350 cm^{-1} shifts by approximately −15 cm^{-1} for K10 and

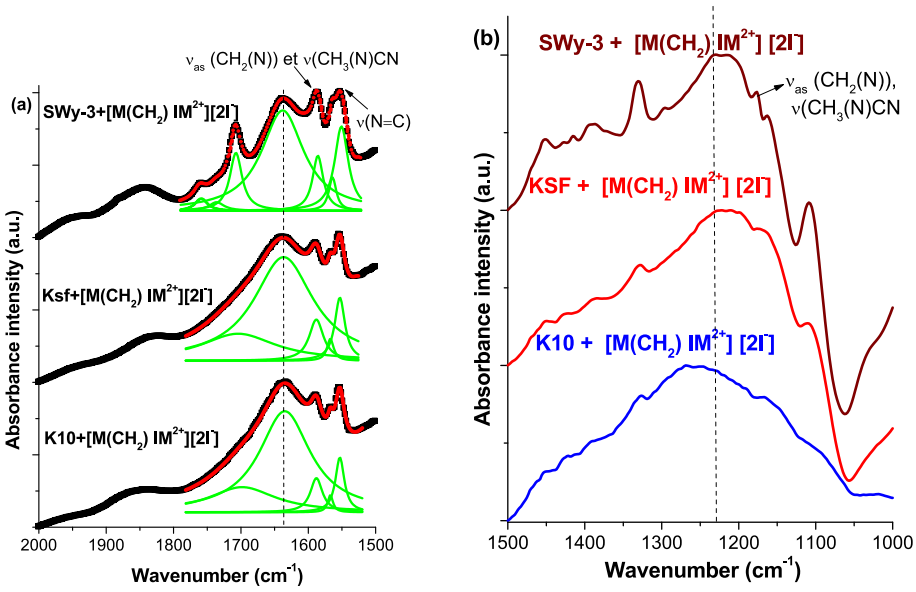

Fig. 13. The HTS/FTIR spectra of K10, KSF, and SWy-3 modified with $[M(CH_2)IM^{2+}][2I^-]$ in the spectral range (a) 2000–1500 cm^{-1} (the black dashed line represents the mode at 1635 cm^{-1}) and (b) 1500–1000 cm^{-1} (the black dashed line represents the mode at 1235 cm^{-1}). The green curves correspond to the fitting of the vibrational modes in this spectral region using Lorentzian functions. The red curve corresponds to the overall fit; it is noted that this curve closely matches the experimental black curve. (For interpretation of the references to colour in this figure legend, the reader is referred to the web version of this article.)

Table 11
Intensity ratios of several peaks of K10, KSF, and SWy-3 modified by [M (CH_2) IM^{2+}] [$2I^-$] in the spectral range of 3800–2600 cm^{-1}.

Modified Clays	I_{3420}/I_{3625} $[M(CH_2)IM^{2+}][2I^-]$	I_{3160}/I_{3115} $[M(CH_2)IM^{2+}][2I^-]$
K10	0.97 ± 0.02	1.05 ± 0.02
KSF	0.90 ± 0.02	1.04 ± 0.02
SWy-3	0.84 ± 0.02	0.97 ± 0.02

Table 12
Intensity ratios of various peaks of K10, KSF, SWy-3 modified by the ionic liquid $[M(CH_2)IM^{2+}]$ [$2I^-$] in the spectral domain 2000–1000 cm^{-1}.

Modified Clays	I_{1850}/I_{1633} $[M(CH_2)IM^{2+}]$ [$2I^-$]	I_{1633}/I_{1250} $[M(CH_2)IM^{2+}]$ [$2I^-$]	I_{1105}/I_{1250} $[M(CH_2)IM^{2+}]$ [$2I^-$]
K10	0.26 ± 0.02	0.67 ± 0.02	0.71 ± 0.02
KSF	0.31 ± 0.02	0.61 ± 0.02	0.62 ± 0.02
SWy-3	0.37 ± 0.02	0.68 ± 0.02	0.45 ± 0.02

KSF, displaying the same phenomenon in the same proportion, whereas for modified SWy-3, it shifts by approximately −20 cm^{-1}.

We also note a significant shift for a mode assigned to the stretching vibration ν(O—H) at 1250 cm^{-1}, with a shift of approximately −15 cm^{-1} for modified K10 and KSF, while for modified SWy-3, the shift is even more pronounced, around −35 cm^{-1}. The peak at 1164 cm^{-1}, assigned to the νas(CH_2(N)) and ν(CH_3(N)) CN modes for $[M(CH_2)IM^{2+}][2I^-]$, shifts to 1168 and 1160 cm^{-1} for modified K10 and KSF, while for modified SWy-3, it splits into two peaks at 1176 and 1163 cm^{-1}.

3.4. Summary of vibrational differentiation markers

We observed different vibrational behaviors between K10, KSF, and SWy-3 modified by the same ionic liquid. These differences were evident in changes in intensity, peak shifts, and the appearance of new peaks.

In the spectral range 3800–2600 cm^{-1}, shown in Fig. 6, we observed a similar phenomenon with a significant increase in intensity for the mode assigned to the stretching vibrations ν(N—H) and ν(C—H) in the spectral range of 3200–2900 cm^{-1} for SWy-3 modified by $[EMIM^+][I^-]$, compared to K10 and KSF modified. In Fig. 10, we observed a difference in spectral richness related to the choice of clay. In the 3100–2850 cm^{-1} range, $[M(CH_2)IM^{2+}][2I^-]$ appeared to interact more effectively with SWy-3 than with K10 and KSF: we observed two intensity doublets at 3073, 3050 cm^{-1} and 2883, 2868 cm^{-1} for modified SWy-3, whereas these were not present in the spectra of modified K10 and KSF.

In the spectral range 2000–1000 cm^{-1}, particularly in the 2000–1500 cm^{-1} range (Fig. 7.a), we noted a difference in spectral richness between K10, KSF, and SWy-3 modified: two significant intensity doublets at 1651, 1621 cm^{-1} and 1583, 1565 cm^{-1} for SWy-3 modified by $[EMIM^+][I^-]$, while only two peaks were observed for K10 and KSF modified by $[EMIM^+][I^-]$ at 1639 cm^{-1} (corresponding to the vibrational modes δ(OH), ν(C=C), ν(N=C-N)) and at 1574 cm^{-1} (corresponding to the vibrational modes ν(CH_2(N)), ν(CH_3(N)CN)). However, in the 1500–1000 cm^{-1} range, we observed a similar phenomenon for all three modified clays with frequency shifts: the peaks at 1250 cm^{-1} and 1105 cm^{-1} for K10, KSF, and SWy-3 modified by $[EMIM^+][I^-]$. In Fig. 11.a, we observed two significant intensity peaks for SWy-3 modified by $[M(CH_2)IM^{2+}][2I^-]$ that were not present in the other two cases: 1756 and 1707 cm^{-1}, which were assigned to δ(OH) and ν(C=C-H). In the 1500–1300 cm^{-1} range, the peaks in the spectrum of SWy-3 modified by $[M(CH_2)IM^{2+}][2I^-]$ were more pronounced than those in the spectra of K10 and KSF modified by $[M(CH_2)IM^{2+}][2I^-]$. We observed a frequency shift for the peaks at 1581, 1558, and 1543 cm^{-1}: they shifted to 1587, 1567, and 1550 cm^{-1} for K10 and KSF modified. In the 1500–1000 cm^{-1} region (Fig. 11b), we observed a difference in spectral richness: two significant intensity doublets at 1427, 1416 cm^{-1} and 1176, 1163 cm^{-1} for SWy-3 modified by $[M(CH_2)IM^{2+}][2I^-]$, whereas only two peaks were observed for K10 and KSF modified at 1425 cm^{-1} (corresponding to the vibrational modes δ(OH), ν(CH_2(N)), ν(CH_3(N)CN)) and at 1565 cm^{-1} (corresponding to the vibrational modes ν(CH_2(N)) and ν(CH_3(N))).

4. Conclusions

The study of the porosity of the three clays by the BET method revealed significant differences between them. The measurement of the specific adsorption surface area (SBET) is much higher for

montmorillonite K10 (S_{BET} = 280 cm^2/g) compared to the other two montmorillonites, KSF (S_{BET} = 97 cm^2/g) and SWy-3 (S_{BET} = 45 cm^2/g). This variation in the specific surface area value is related to the different treatments applied to each clay. The application of a strong sulfuric acid treatment to montmorillonite significantly increased the adsorption surface area for K10. A less concentrated treatment for montmorillonite KSF limited its adsorption capacity. For SWy-3, the difference in behavior is likely due to its high sodium content. Apparently, the presence of these Na^+ ions in the clay structure does not favor significant adsorption. It is also noteworthy that for montmorillonite K10, the distribution of pore diameters is broader than for the other two montmorillonites, leading us to believe that water molecules are more present on the external surface compared to the other two clays, for which water molecules are almost exclusively in the interstitial space.

For montmorillonite K10, S_{BET} decreases from 280 m^2/g to 91 m^2/g with the addition of [M(CH_2) IM^{2+}][$2I^-$]. This decrease in the specific surface area is also accompanied by a drop in pore volumes and a widening of the pore size distribution. This led us to believe that the ionic liquid molecules are primarily in the interstitial space, but also partly on the external surface of the modified clay. The case of montmorillonite KSF is particular compared to the other two montmorillonites. Indeed, the KSF + [M(CH_2) IM^{2+}][$2I^-$] mixture has a very slightly lower specific surface area than that of the pure clay: it decreases from 97 m^2/g to 91 m^2/g, with the pore volume and pore diameter remaining constant, without any widening of the pore size distribution. This mixture seems to be the ideal candidate for the treatment of toxic waste since the ionic liquid molecules are found only in the interstitial space, with still available space to capture pollutant molecules. The mixtures with montmorillonite SWy-3 modified by the [M(CH_2) IM^{2+}][$2I^-$] ionic liquid is quite unique: we observe a very significant decrease in the specific surface area S_{BET}: it decreases from 45 m^2/g to 3 m^2/g with the I-anion, with a significant widening of the pore size distribution. It thus seems that the dicationic ionic liquid occupies almost all of the interstitial space and also part of the external surface of the modified clay for this case.

Through HTS/FTIR investigations, we demonstrated the specific vibrational behavior of purified and modified SWy-3 by studying various modes: δ(OH), ν(CH_2(N)), ν(CH_3(N)CN)), ν(O—H), δ(CH_2), and ν(CCH). By comparing the spectra of purified K10, KSF, and SWy-3 MMTs, we observed the appearance of new peaks and significant variations in intensity between the clays, depending on the type of ionic liquid chosen. These vibrational changes were directly related to the presence of ionic liquids in the clays. The dicationic ionic liquid [M(CH_2)IM^{2+}][$2I^-$] exhibited a richer spectral response than the monocationic ionic liquid in all three clays, with SWy-3 MMT being more vibrational changes to both monocationic and dicationic ionic liquids than K10 and KSF MMTs. These studies revealed that the introduction of ionic liquids into clays has a direct impact on the infrared spectra, with the existence of vibrational markers.

Disclaimer/Publisher's note

The statements, opinions and data contained in all publications are solely those of the individual author(s) and contributor(s) and not of the editor(s). The editor(s) disclaim responsibility for any injury to people or property resulting from any ideas, methods, instructions or products referred to in the content.

CRediT authorship contribution statement

A. Ahmed: Writing – original draft, Investigation, Conceptualization. **W.A.A. Ahmed:** Investigation. **T. Moumene:** Methodology. **El H. Belarbi:** Resources, Methodology. **V. Baeten:** Resources. **S. Bresson:** Supervision, Investigation, Conceptualization.

Informed consent statement

Not applicable.

Institutional review board statement

Not applicable.

Funding

This research did not receive any specific grant from funding agencies in the public, commercial, or not-for-profit sectors.

Declaration of competing interest

The authors declare that they have no known competing financial interests or personal relationships that could have influenced the work reported in this paper.

Acknowledgments

we would like to thank Quentin Arnould, technician at Wallon Agricultural Research Centre (CRA-W), who participated in the HTS/FTIR measurements.

Data availability

Data will be made available on request.

References

[1] N. Yaghmaeiyann, M. Mirzaei, R. Delghavi, Montmorillonite clay: introduction and evaluation of its applications in different organic syntheses as catalyst: a review, Results Chem. 4 (2022) 100549, https://doi.org/10.1016/j.rechem.2022.100549.
[2] J.A. Fiscal-Ladino, M. Obando-Ceballos, M. Rosero-Moreano, Ionic liquids intercalated in montmorillonite as the sorptive phase for the extraction of low-polarity organic compounds from water by rotating-disk sorptive extraction, Anal. Chim. Acta 953 (2017) 23–31, https://doi.org/10.1016/j.aca.2016.10.009.
[3] C. Takahashi, T. Shirai, M. Fuji, Study on intercalation of ionic liquid into montmorillonite and its property evaluation, Mater. Chem. Phys. 135 (2–3) (2012) 681–686, https://doi.org/10.1016/j.matchemphys.2012.05.044.
[4] E. Kianfar, S. Mafi, Ionic liquids: properties, application, and synthesis, Fine Chem. Eng. 2 (1) (2021) 21–29, https://doi.org/10.37256/fce.212021693.
[5] O. Bourbigou, H. Magna, D. Morvan, Ionic liquids and catalysis: recent progress from knowledge to applications, Appl. Catal. Gen. 373 (1–2) (2010) 1–56, https://doi.org/10.1016/j.apcata.2009.10.008.
[6] S.S. De Jesus, R. Maciel Filho, Are ionic liquids eco-friendly? Renew. Sustain. Energy Rev. 157 (2022) 112039 https://doi.org/10.1016/j.rser.2021.112039.
[7] R.A. Khan, M. Murtaza, A. Abdulraheem, Imidazolium-based ionic liquids as clay swelling inhibitors: mechanism, performance evaluation, and effect of different anions, ACS Omega 5 (41) (2020) 26682–26696, https://doi.org/10.1021/acsomega.0c03560.
[8] A. Ahmed, Y. Chacker, El H. Belarbi, et al., XRD and ATR/FTIR investigations of various montmorillonite clays modified by monocationic and dicationic imidazolium ionic liquids, J. Mol. Struct. 1173 (2018) 653–654, https://doi.org/10.1016/j.molstruc.2018.07.066.
[9] T. Moumene, E.H. Belarbi, B. Haddad, D. Villemin, O. Abbas, B. Khelifa, S. Bresson, Vibrational spectroscopic study of ionic liquids: comparison between monocationic and dicationic imidazolium ionic liquids, J. Mol. Struct. 1065 (2014) 86–92, https://doi.org/10.1016/j.molstruc.2014.02.034.
[10] L.P. Lavikainen, J.T. Tanskanen, T. Schatz, S. Kasa, T.A. Pakknen, Montmorillonite interlayer surface chemistry: effect of magnesium ion substitution on cation adsorption, Theor. Chem. Acc. 134 (2015) 1–7, https://doi.org/10.1007/s00214-015-1666-1.
[11] D.F. Montano, H. Casanova, W.I. Cardona, L.F. Giraldo, Functionalization of montmorillionite with ionic liquids based on 1-alkyl-3-methylimidazolium: effect of anion and length chain, Mater. Chem. Phys. 198 (2017) 386–392, https://doi.org/10.1016/j.matchemphys.2017.06.027.
[12] J.A. Fiscal-Ladino, M. Obando-Ceballos, M. Rosero-Moreano, D.F. Montano, W. Cardona, L.F. Giraldo, P. Ritcher, Ionic liquids intercalated in montmorillonite as the sorptive phase for extraction of low-polarity organic compounds from water by rotating-disk sorptive extraction, Anal. Chim. Acta 953 (2017) 23–31, https://doi.org/10.1016/j.aca.2016.11.067.
[13] J. Holly, P.M. Brennan, J.M. Cameron, et al., Development of high-throughput ATR-FTIR technology for rapid triage of brain cancer, Nat. Commun. 10 (1) (2019) 4501, https://doi.org/10.1038/s41467-019-12527-5.

[14] G. Jozanikohan, M.N. Abarghooei, The Fourier transform infrared spectroscopy (FTIR) analysis for the clay mineralogy studies in a clastic reservoir, J. Petrol. Explor. Prod. Technol. 12 (8) (2022) 2093–2106, https://doi.org/10.1007/s13202-021-01449-y.
[15] F. Bergaya, R.P. Chicinas, H. Bedelean, R. Stefan, A. Maicaneanu, Ability of a montmorillonitic clay to interact with cationic and anionic dyes in aqueous solutions, J. Mol. Struct. 1154 (2018) 187–195, https://doi.org/10.1016/j.molstruc.2017.10.038.
[16] M.D. Donohue, G.L. Aranovich, Classification of Gibbs adsorption isotherms, Adv. Colloid Interface Sci. 76 (1998) 137–152, https://doi.org/10.1016/S0001-8686(98)00044-X.
[17] A. Haouzi, M. Kharroubi, El H. Belarbi, S. Devautour-Vinot, F. Henn, J.C. Giuntini, Activation energy for dc conductivity in dehydrated alkali metal-exchanged montmorillonites experimental results and model, Appl. Clay Sci. 27 (2004) 67–74, https://doi.org/10.1016/j.clay.2003.08.001.
[18] K. Noack, P.S. Schulz, N. Paape, J. Kiefer, P. Wasserscheid, A. Leipertz, The role of the C2 position in interionic interactions of imidazolium based ionic liquids: a vibrational and NMR spectroscopy study, Phys. Chem. Chem. Phys. 12 (2010) 14153–14161, https://doi.org/10.1039/C0CP00486C.
[19] S. Kawi, Y.Z. Yao, Silica bonded K10 montmorillonite (SBM): a high surface area catalytic clay material, Microporous Mesoporous Mater. 28 (1999) 25–34, https://doi.org/10.1016/S1387-1811(98)00279-0.
[20] P. Bühlmann, E. Pretsch, Structure Determination of Organic Compounds, 4th Revised and Enlarged Ed, Springer-Verlag, Berlin Heidelberg, 2009. ISBN 978-3-662-04201-4.
[21] Y. Chaker, H. Ilikti, M. Debdab, T. Moumene, E.H. Belarbi, A. Wadouachi, O. Abbas, B. Khelifa, S. Bresson, Synthesis and characterization of 1-(hydroxyethyl)-3-methylimidazolium sulfate and chloride ionic liquids, J. Mol. Struct. 1113 (2016) 182–190, https://doi.org/10.1016/j.molstruc.2016.02.017.
[22] T. Moumene, E.H. Belarbi, B. Haddad, D. Villemin, O. Abbas, B. Khelifa, S. Bresson, Vibrational spectroscopic study of imidazolium dicationic ionic liquids: effect of cation alkyl chain length, J. Appl. Spectrosc. 83 (12) (2016) 165–171, https://doi.org/10.1007/s10812-016-0264-7.
[23] G. Mathias, D. Marx, Structures and spectral signatures of protonated water networks in bacteriorhodopsin, Pro. Natl. Acad. Sci. U.S.A. 104 (17) (2007) 6980–6985, https://doi.org/10.1073/pnas.0609229104.
[24] J. Madejova, P. Komadel, Baseline studies of the clay minerals society source clays: infrared methods, Clay Clay Miner. 49 (15) (2001) 410–432, https://doi.org/10.1346/CCMN.2001.0490508.
[25] C.T. Johnston, S.P. Gnanasiri, Polarized ATR-FTIR study of smectite in aqueous suspension, Langmuir 17 (2001) 3712–3718, https://doi.org/10.1021/la010086g.
[26] J. Madejova, FTIR techniques in clay mineral studies, Vib. Spectrosc. 3 (2003) 1–10, https://doi.org/10.1016/S0924-2031(02)00065-6.
[27] G. Socrates. Infrared and Raman Characteristic Group Frequencies: Tables and Charts. John Wiley & Sons, New York, USA 2004. ISBN 0–470–09307-2.
[28] T. Moumene, E.H. Belarbi, B. Haddad, D. Villemin, O. Abbas, B. Khelifa, S. Bresson, Study of imidazolium dicationic ionic liquids by Raman and FTIR spectroscopies: the effect of the nature of the anion, J. Mol. Struct. 1083 (2015) 179–186, https://doi.org/10.1016/j.molstruc.2014.11.061.
[29] L. Wu, L. Liao, G. Lv, F. Qin, Z. Li, Microstructure and process of intercalation of imidazolium ionic liquids into montmorillonite, Chem. Eng. J. 236 (2014) 306–313, https://doi.org/10.1016/j.cej.2013.09.063.
[30] H.-C. Kan, M.-C. Tseng, Y.-H. Chu, Bicyclic imidazolium-based ionic liquids: synthesis and characterization, Tetrahedron 63 (7) (2007) 1644–1653, https://doi.org/10.1016/j.tet.2006.12.003.